Rare Metal Materials and Engineering
Volume 55, Issue 5, May 2026
Available online at www.rmme.ac.cn

Science Press

Cite this article as: Ou Pengcheng, Wan Qiang, Jiang Hui, et al. Effect of Element Ti on Microstructure, Properties, and Thermal Stability of $NbTaMoWTi_x$ Refractory High-Entropy Alloys[J]. Rare Metal Materials and Engineering, 2026, 55(05): 1184-1190. DOI: https://doi.org/10.12442/j.issn.1002-185X.20250034.

ARTICLE

Effect of Element Ti on Microstructure, Properties, and Thermal Stability of $NbTaMoWTi_x$ Refractory High-Entropy Alloys

Ou Pengcheng[1], Wan Qiang[1], Jiang Hui[2], Sha Minghong[1], Sun Jiabin[1], Ai Xingang[1], Li Shengli[1], Huang Tiandang[1]

[1] School of Materials and Metallurgy, University of Science and Technology Liaoning, Anshan 114051, China; [2] College of Mechanical and Electronic Engineering, Qingdao University, Qingdao 266000, China

Abstract: The effect of element Ti on the microstructures and mechanical properties of as-cast and annealed $NbTaMoWTi_x$ (x=0, 1, 1.5, 2) refractory high-entropy alloys (RHEAs) was investigated. Results show that after Ti addition, the as-cast alloys maintain their original single body-centered cubic (bcc) structure. As for the mechanical properties, compared with those without Ti addition, the strength and ductility of $NbTaMoWTi_x$ alloys increase by 93% and 215%, respectively. Furthermore, the $NbTaMoWTi_x$ alloys exhibit outstanding thermal stability. After annealing at 1400 °C, they still maintain the single bcc structure, and their mechanical properties are even slightly improved. However, annealing leads to a significant deterioration in the mechanical properties of high-Ti-content alloys ($NbTaMoWTi_{1.5}$ and $NbTaMoWTi_2$), owing to the formation of Ti-rich acicular phases.

Key words: high-entropy alloys; refractory alloy; titanium; mechanical properties; thermal stability

1 Introduction

High-entropy alloys (HEAs) [1], or multi-principal-element alloys[2], have emerged as metallic materials with great application potential[3] due to their unique structures[4] and excellent properties, such as strength, ductility[5–7], oxidation resistance[8], thermal stability[9–10], wear resistance[11], and resistivity[12]. Refractory high-entropy alloys (RHEAs) [13], a prominent subset of HEAs, generally contain refractory elements, such as Hf[14], Mo[15], Nb[16], Ta[17], Ti[18], V[19], W[20], and Zr[21]. Owing to the high melting points of their constituent elements, most RHEAs also exhibit high melting points and outstanding mechanical properties at elevated temperatures[22]. Among existing RHEAs, NbTaMoW alloy has shown particular promise for widespread industrial applications at temperatures over 1000 °C[23–26].

However, refractory alloys containing elements from group V (V, Nb, and Ta) and group VI (Cr, Mo, and W) possess certain disadvantages, such as poor ductility at room temperature. For instance, the compressive ductility of NbTaMoW alloy is below 3%[22], severely restricting its applicability. Consequently, enhancing the ductility of NbTaMoW alloy remains a key challenge in industry.

The high ductility and excellent mechanical properties of Ti-based alloys at elevated temperatures have been well-studied, and their substantial application potential in many industrial fields has been frequently demonstrated. In this regard, Ti is an important component of numerous RHEAs[18,25–27]. Additionally, as an element of group IV, Ti can effectively reduce the average valence electron concentration (VEC) of alloys composed of elements from group V and group VI, and thereby improve their ductility.

In this research, Ti was added into NbTaMoW alloy to form

Received date: May 16, 2025
Foundation item: National Natural Science Foundation of China (51774179); Natural Science Foundation of Liaoning Province (20180550546); Joint Fund of State Key Laboratory of Metal Material for Marine Equipment and Application (HGSKL-USTLN(2021)03); High-Level Talent Fund of USTL (6003000377, 6003000294); supported by Liaoning Provincial Department of Education (LJ212410146037)
Corresponding author: Huang Tiandang, Ph. D., School of Materials and Metallurgy, University of Science and Technology Liaoning, Anshan 114051, P. R. China, E-mail: huangtiandang@ustl.edu.cn

a new series of NbTaMoWTi$_x$ RHEAs. Both the as-cast and annealed NbTaMoWTi$_x$ RHEAs demonstrated enhanced ductility and strength while maintaining their original single-phase body-centered cubic (bcc) structure.

2 Experiment

Raw materials (Nb, Ta, Mo, W, V, and Ti) with purities exceeding 99.99wt% were used to prepare NbTaMoWTi$_x$ alloys in this research. NbTaMoWTi$_x$ alloys with x=0, 1, 1.5, and 2 were denoted as Ti00, Ti10, Ti15, and Ti20 alloys, respectively. The alloys were melted via vacuum arc melting. Before melting, the chamber was evacuated to 3×10^{-3} Pa and subsequently backfilled with high-purity argon to 0.05 Pa. All alloy samples were remelted at least 8 times to ensure homogeneity and solidification in a water-cooled copper hearth. The crystal structures of the alloys were identified using X-ray diffractometer (XRD, EMPYREAN). Scans were performed at 2θ =20° – 100° at a speed of 0.216°/s. The microstructure and phase composition of the alloys were analyzed using a JXA-8530F PLUS electron probe microanalysis (EPMA) equipped with X-ray wavelength dispersive spectroscope (WDS). Vickers hardness measurements were performed using an MH-50 hardness tester under the load of 500 g for 15 s. The mechanical properties were measured using a DNS-100 uniaxial compression tester. The compressive samples were cylindrical (diameter: 5 mm; height: 10 mm). The strain rate used for all the mechanical property tests was 1×10^{-3} s^{-1}. Annealing treatments were conducted in a vacuum tube furnace. Samples were heated to 1400 °C at heating rate of 10 K/s and held at this temperature for 12 h.

3 Results and Discussion

Fig. 1 shows XRD patterns of the as-cast NbTaMoWTi$_x$ alloys. All alloys exhibit typical single-phase bcc structure. VEC values of the Ti00, Ti10, Ti15, and Ti20 alloys are 5.5, 5.2, 5.1, and 5.0, respectively, indicating that all alloys have the bcc structure[28].

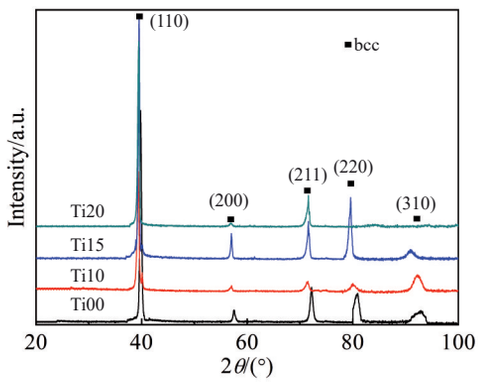

Fig.1 XRD patterns of as-cast NbTaMoWTi$_x$ alloys

Diffraction peaks shift towards lower angle region with the increase in Ti content, indicating the lattice expansion. The lattice constants of the Ti00, Ti10, Ti15, and Ti20 alloys are 0.320 32, 0.322 74, 0.323 12, and 0.323 18 nm, respectively, further confirming the lattice expansion. This phenomenon is attributed to the fact that the atomic radius of Ti (147 pm) is larger than the average atomic radius of the Ti00 alloy (144 pm). Thus, the average atomic radii of the NbTaMoWTi$_x$ alloys are increased with the increase in Ti content, resulting in the lattice expansion.

Fig. 2 shows EPMA images of the as-cast NbTaMoWTi$_x$ alloys. All alloys exhibit typical dendrite structures. Based on the imaging principle of EPMA, it can be inferred that elemental segregation occurs in the NbTaMoWTi$_x$ alloys. According to WDS results listed in Table 1, the light region (dendrite region, denoted as DR) is enriched in elements W

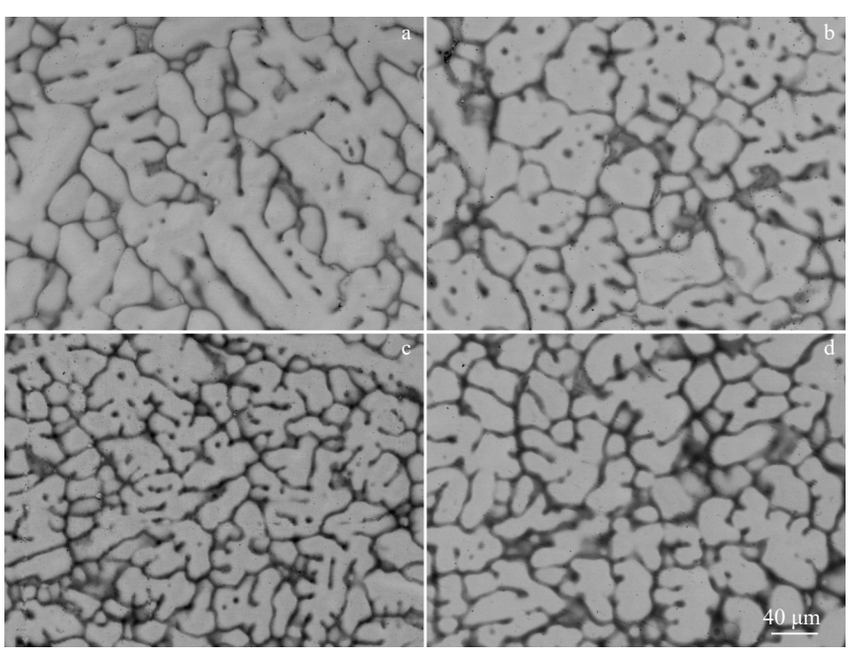

Fig.2 EPMA images of as-cast NbTaMoWTi$_x$ alloys: (a) Ti00, (b) Ti10, (c) Ti15, and (d) Ti20

Table 1 WDS results of as-cast NbTaMoWTi$_x$ alloys (at%)

Alloy	Region	Nb	Ta	Mo	W	Ti
Ti00	DR	19.76	25.68	21.80	33.43	-
	ID	32.81	29.16	27.29	17.76	-
Ti10	DR	18.90	23.40	16.92	26.95	13.83
	ID	24.92	14.89	17.34	9.71	33.13
Ti15	DR	16.96	21.40	18.02	24.85	18.76
	ID	18.24	9.46	15.61	5.23	49.85
Ti20	DR	16.59	19.68	16.42	21.47	25.83
	ID	17.37	10.16	14.55	6.91	51.00

and Ta. The dark region (interdendritic region, denoted as ID) is enriched in elements Nb and Mo for the Ti00 alloy and enriched in elements Nb, Mo, and Ti for the Ti10, Ti15, and Ti20 alloys. This segregation follows the solidification sequence: elements with higher melting points (W, Ta) solidify earlier in DR, whereas the lower-melting-point elements, such as Ti, are concentrated in ID during solidification. The rapid cooling during vacuum arc melting further exacerbates this effect. WDS element mapping results of the as-cast Ti15 alloy are shown in Fig.3.

Fig. 4 shows the Vickers hardness results of the as-cast NbTaMoWTi$_x$ alloys. Vickers hardness is increased initially but then decreased with the increase in Ti addition. This trend

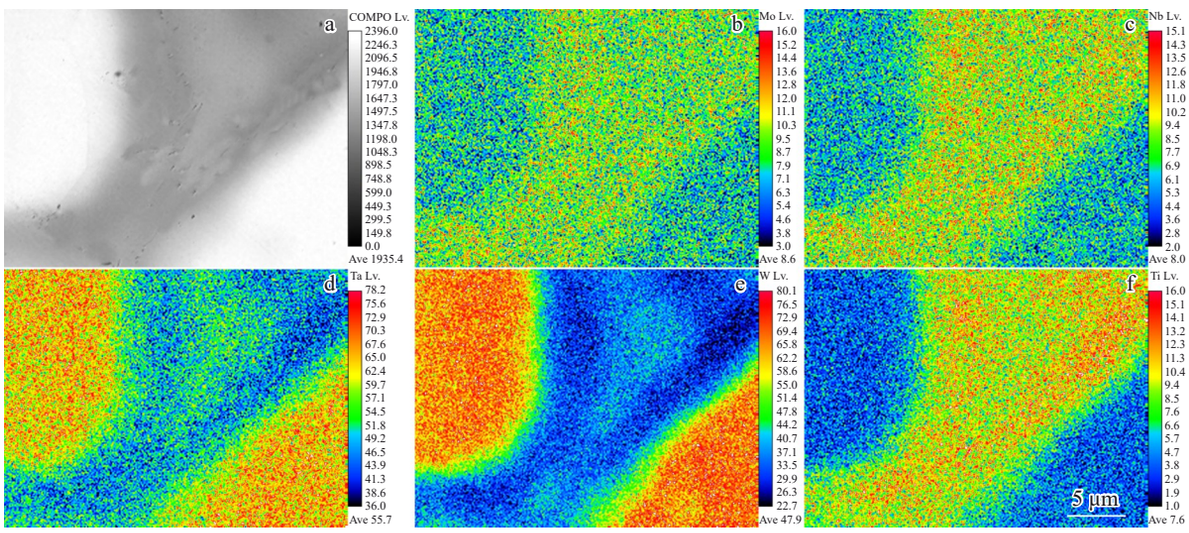

Fig.3 WDS element mapping results of as-cast Ti15 alloy: (a) composite; (b) Mo; (c) Nb; (d) Ta; (e) W; (f) Ti

can be explained by two competing effects: (1) solid solution strengthening caused by multi-component mixing; (2) degraded solid solution strengthening effect resulting from reduced atomic radius mismatch (Ti00: 2.82%, Ti10: 2.65%, Ti15: 2.56%, and Ti20: 2.49%). Additionally, the inherent low hardness of Ti contributes to the decline in hardness at high Ti contents.

Fig. 5 displays the compressive engineering stress-engineering strain curves of the as-cast NbTaMoWTi$_x$ alloys. The strength and plasticity of the NbTaMoWTi$_x$ alloys are improved after the Ti addition. The fracture strength increases from 1087 MPa (Ti00) to 2101 MPa (Ti20), improved by approximately 93%. Accordingly, the compression plasticity increases from 4.1% (Ti00) to 12.9% (Ti20), improved by 215%. The enhancement is attributed to Ti addition, which reduces VEC value and Fermi energy, promoting shear instability along the <100> tetragonal path under tension[29–30].

The yield strength $\sigma_{0.2}^{cal}$ of HEAs with single bcc structure[31] can be estimated by Eq.(1):

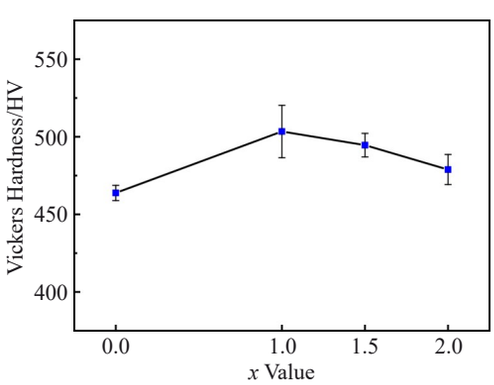

Fig.4 Vickers hardness results of as-cast NbTaMoWTi$_x$ alloys

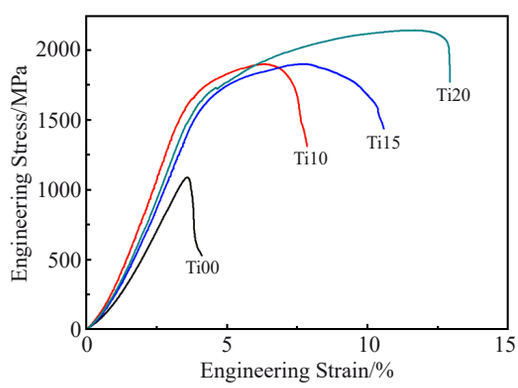

Fig.5 Compressive engineering stress-engineering strain curves of as-cast NbTaMoWTi$_x$ alloys

$$\sigma_{0.2}^{cal} = N(\sigma_{0.2}^{mix} + \Delta\sigma) \quad (1)$$

where N is a constant (N=0.9), $\sigma_{0.2}^{mix}$ is the yield strength of the alloy calculated by the mixing law, and $\Delta\sigma$ is the yield strength produced by the interactions of the alloy components. $\Delta\sigma$ can be calculated by the following equations:

$$\Delta\sigma = (\Sigma\Delta\sigma_i^{3/2})^{2/3} \quad (2)$$

$$\Delta\sigma_i = (AGf_i^{4/3})^{2/3} \quad (3)$$

where $\Delta\sigma_i$ is the yield strength contributed from solution strengthening caused by the ith component; A is a dimensionless constant related to the material; G is the shear modulus of the alloy; f_i is the mismatch coefficient of the ith component[30]. The theoretical yield strength of the $NbTaMoWTi_x$ alloys calculated by Eq.(1–3) is listed in Table 2. For the Ti00 alloy, it is found that there is a large gap between the calculated yield strength and the measured one, which may be attributed to the casting defects caused by the inferior fluidity of the alloy, as well as the casting stress. However, the measured yield strength values of Ti-containing Ti10, Ti15, and Ti20 alloys are close to their calculated ones.

Fig.6 shows the compressive fracture surfaces of the as-cast $NbTaMoWTi_x$ alloys. According to Fig. 6, dendritic structures can be observed in the Ti00 alloy, indicating that transgranular fracture is its main fracture form. This is attributed to the considerably weak bonds between DR and ID, which cause the cracks to expand along the junctions during compression. After the Ti addition, river patterns and tearing edges can be observed in Ti10, Ti15, and Ti20 alloys. Notably, with the increase in Ti content, the fraction corresponding to the dendritic structure is decreased, whereas the river patterns and tearing edges are increased. The main fracture mode changes from transgranular fracture to cleavage. This is also due to the Ti addition which reduces the atomic-size difference in the $NbTaMoWTi_x$ alloys. Moreover, Ti acts as an adhesive to strengthen the bonds between DR and ID.

Fig. 7 shows XRD patterns of the annealed $NbTaMoWTi_x$ alloys. After annealing at 1400 °C for 12 h, Ti00 and Ti10 alloys retain the bcc structure, whereas Ti15 and Ti20 have bcc+close-packed hexagonal (hcp) dual-phase structures. This transition aligns with the binary Nb-Ti/Mo-Ti phase diagrams, where high Ti content exceeds the solubility limit, inducing hcp phase formation during cooling process. The lower mixing enthalpy of Mo-Ti (−4 kJ/mol), compared with that of Nb-Ti (2 kJ/mol), explains the preferential Mo-Ti interaction in Ti10 alloy, stabilizing its bcc phase.

Fig. 8 shows EPMA images of the annealed $NbTaMoWTi_x$ alloys. An obvious homogenization can be observed. In Ti00 and Ti10 alloys, particularly, the boundaries between DR and ID become very blurred. The homogenization depends on the content of Ti which decreases the lattice constant and aggravates the sluggish diffusion effect. In addition, a Ti-rich acicular phase can be observed in ID of the Ti15 and Ti20 alloys, and its volume fraction is increased with the increase

Table 2 Mechanical properties of as-cast $NbTaMoWTi_x$ alloys

Alloy	Vickers hardness/HV	Theoretical yield strength/MPa	Measured yield strength/MPa	Fracture strength/MPa	Compressive ductility/%
Ti00	464	1481	1065	1087	4.1
Ti10	503	1589	1586	1897	7.9
T15	495	1536	1565	1900	10.6
Ti20	488	1517	1514	2101	12.9

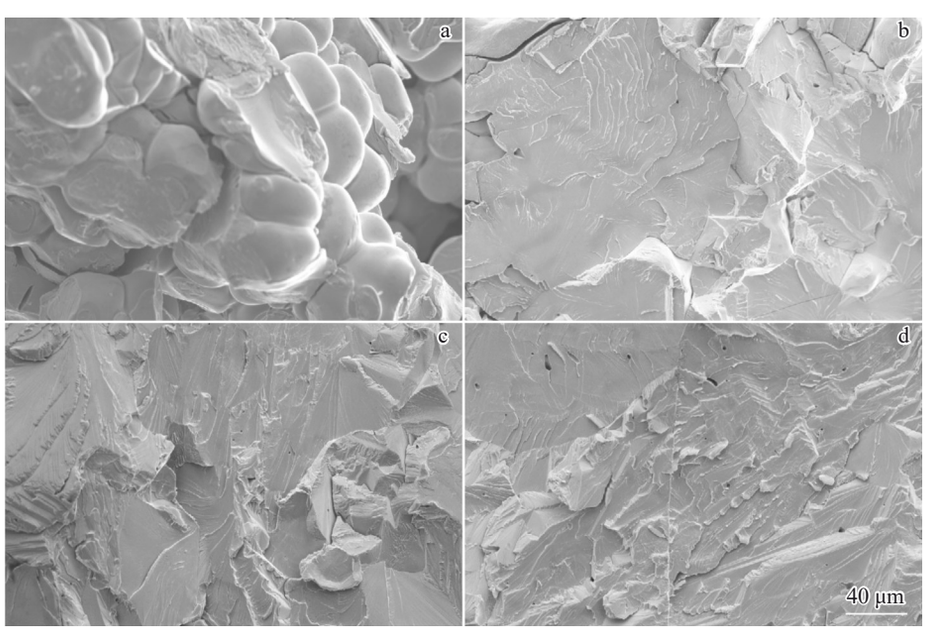

Fig.6 EPMA images of compressive fracture surfaces of as-cast $NbTaMoWTi_x$ alloys: (a) Ti00, (b) Ti10, (c) Ti15, and (d) Ti20

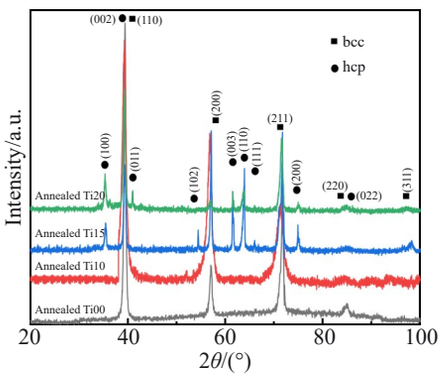

Fig.7 XRD patterns of annealed NbTaMoWTi$_x$ alloys

in Ti content. According to WDS results of the annealed NbTaMoWTi$_x$ alloys (Table 3), segregation is mitigated in the Ti00 and Ti10 alloys. Specifically, for the Ti15 and Ti20 alloys, Ti is the major component of the Ti-rich acicular phase with the atomic fraction exceeding 80%.

Fig. 9 shows the Vickers hardness results of the annealed NbTaMoWTi$_x$ alloys. In contrast to those of the as-cast alloys, the Vickers hardness of the annealed alloys first increases and then decreases. However, after annealing, the Vickers hardness of NbTaMoWTi$_x$ alloys only exhibits an increasing trend with the increase in Ti content. Although that of the Ti00 and Ti10 alloys changes slightly after annealing, the Vickers hardness of the Ti15 and Ti20 alloys significantly increases. This phenomenon is attributed to the formation of the hard Ti-rich phase.

Fig. 10 shows the compressive engineering stress-engineering strain curves of the annealed NbTaMoWTi$_x$ alloys. After annealing treatment, the ductility of the Ti15 and Ti20 alloys decreases significantly, which is obviously caused by the presence of acicular precipitates. On the contrary, the ductility of Ti00 and Ti10 alloys increases after annealing treatment, which is caused by the homogenization during the annealing process. In addition, the strength of Ti00 alloy increases after annealing treatment, which may be caused by the release of casting stress. Table 4 shows the mechanical properties of annealed NbTaMoWTi$_x$ alloys. Among all these

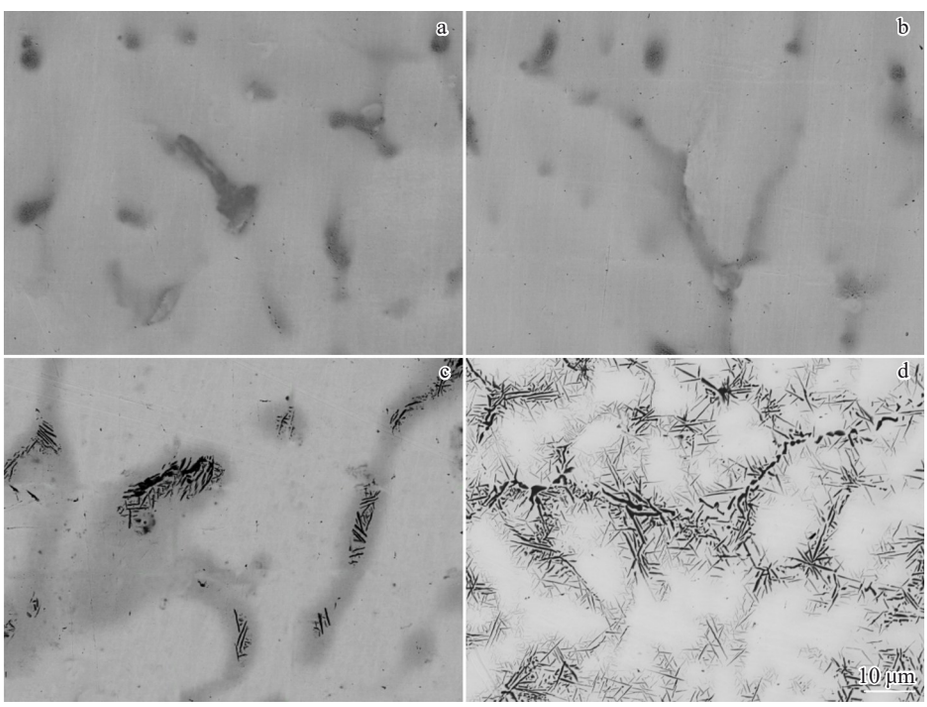

Fig.8 EPMA images of annealed NbTaMoWTi$_x$ alloys: (a) Ti00, (b) Ti10, (c) Ti15, and (d) Ti20

Table 3 WDS results of annealed NbTaMoWTi$_x$ alloys (at%)

Alloy	Region	Nb	Ta	Mo	W	Ti
Ti00	DR	21.63	24.87	22.56	30.94	-
	ID	23.98	24.44	24.09	27.48	-
Ti10	DR	20.59	21.86	17.84	24.15	15.55
	ID	24.78	15.25	17.69	11.78	30.50
Ti15	DR	20.88	17.61	17.31	9.06	35.14
	ID	5.10	4.36	3.74	2.67	84.13
Ti20	DR	18.76	16.53	16.58	6.46	41.67
	ID	4.67	4.95	0.66	0.37	89.34

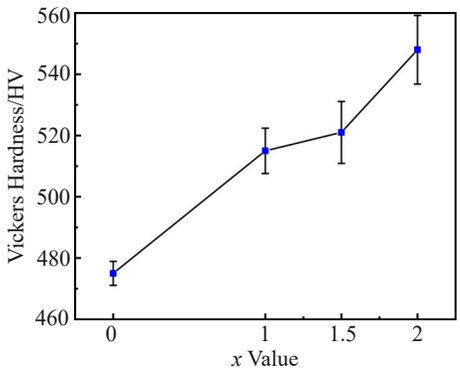

Fig.9 Vickers hardness results of annealed NbTaMoWTi$_x$ alloys

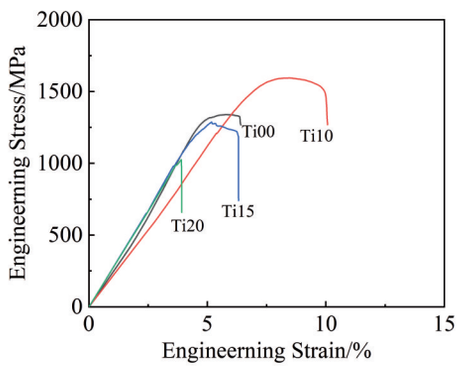

Fig.10 Compressive engineering stress-engineering strain curves of annealed NbTaMoWTi$_x$ alloys

Table 4 Mechanical properties of annealed NbTaMoWTi$_x$ alloys

Alloy	Vickers hardness/HV	Yield strength/MPa	Fracture strength/MPa	Compressive ductility/%
Ti00	475	1293	1318	6.4
Ti10	515	1365	1594	10.0
Ti15	521	1153	1276	6.4
Ti20	548	-	1025	3.9

alloys, the Ti10 alloy displays the optimal mechanical properties after annealing treatment, i.e., the optimal thermal stability.

4 Conclusions

1) The as-cast NbTaMoWTi$_x$ alloys exhibit a single-phase bcc structure with lattice constants increasing linearly from 0.320 32 nm (Ti00) to 0.323 18 nm (Ti20) due to the larger atomic radius of Ti.

2) Elemental segregation occurs in dendritic (W/Ta-rich) and interdendritic (Nb/Mo-rich for Ti00 alloy; Nb/Mo/Ti-rich for Ti10, Ti15, and Ti20 alloys) regions, which is exacerbated by rapid solidification during vacuum arc melting.

3) The mechanical properties are enhanced via Ti addition, i.e., compressive ductility is improved by 215% and fracture strength is improved by 93%. This enhancement is attributed to the reduced VEC value, promoting shear instability along <100> path.

4) After annealing at 1400 °C, Ti00 and Ti10 alloys retain their single-phase bcc structure, whereas the Ti-rich acicular phases form in the Ti15 and Ti20 alloys.

5) Among these tested alloys, the Ti10 alloy exhibits the optimal mechanical properties due to the balanced properties, superior thermal stability, and homogenization capability.

References

1 Yeh J W, Chen S K, Lin S J *et al*. *Advanced Engineering Materials*[J], 2004, 6(5): 299

2 Cantor B, Chang I T H, Knight P *et al*. *Materials Science and Engineering A-Structural Materials Properties Microstructure and Processing*[J], 2004, 375: 213

3 Zhang Y, Zuo T T, Tang Z *et al*. *Progress in Materials Science* [J], 2014, 61: 1

4 Jiang H, Qiao D, Jiao W *et al*. *Journal of Materials Science & Technology*[J], 2021, 61: 119

5 Wang M L, Lu Y P, Lan J G *et al*. *Acta Materialia*[J], 2023, 248: 118806

6 Qiao D X, Jiang H, Jiao W N *et al*. *Acta Metallurgica Sinica* (*English Letters*)[J], 2019, 32(8): 925

7 Guo Jiaming, Ni Bingyu, Jiao Zengbao. *Materials China*[J], 2025, 44(1): 31 (in Chinese)

8 Wei Y, Fu Y, Pan Z M *et al*. *International Journal of Minerals, Metallurgy and Materials*[J], 2021, 28(6): 915

9 Sandrine C, Jean-Marc P, Hidemi K. *Rare Metal Materials and Engineering*[J], 2024, 53(1): 1

10 Vaidya M, Guruvidyathri K, Murty B S. *Journal of Alloys and Compounds*[J], 2019, 774: 856

11 Miao J W, Liang H, Zhang A J *et al*. *Tribology International*[J], 2021, 153: 106599

12 Huang T D, Jiang H, Lu Y P *et al*. *Applied Physics A: Materials Science & Processing*[J], 2019, 125(3): 5

13 Miracle D B, Senkov O N A. *Acta Materialia*[J], 2017, 122: 448

14 Wang F, Shi Q, Liu X *et al*. *Rare Metal Materials and Engineering*[J], 2024, 53(12): 3428

15 Sha M H, Wang S, Li S *et al*. *Rare Metal Materials and Engineering*[J], 2023, 52(11): 3685

16 Wang F L, Balbus G H, Xu S Z *et al*. *Science*[J], 2020, 370(6512): 95

17 Soni V, Senkov O N, Gwalani B *et al*. *Scientific Reports*[J], 2018, 8: 8816

18 Huang T D, Wu S Y, Jiang H *et al*. *International Journal of Minerals, Metallurgy and Materials*[J], 2020, 27(10): 1318

19 Long Y, Liang X, Su K *et al*. *Journal of Alloys and Compounds* [J], 2019, 780: 607

20 Miracle D B, Tsai M H, Senkov O N *et al*. *Scripta Materialia*[J], 2020, 187: 445

21 Chen Zhenzhi, Li Huan, Wang Junjie *et al*. *Titanium Industry Progress*[J], 2024, 41(6): 20 (in Chinese)

22 Senkov O N, Wilks G B, Scott J M *et al*. *Intermetallics*[J], 2011,

19(5): 698
23 Feng X B, Zhang J Y, Xia Z R *et al*. *Materials Letters*[J], 2018, 210: 84
24 Zhang J, Hu Y Y, Wei Q Q *et al*. *Journal of Alloys and Compounds*[J], 2020, 827: 154301
25 Han Z D, Chen N, Zhao S F *et al*. *Intermetallics*[J], 2017, 84: 153
26 Wan Y X, Mo J Y, Wang X *et al*. *Acta Metallurgica Sinica* (*English Letters*)[J], 2021, 34(11): 1585
27 Bencze L, Hasemann G, Sergeev D *et al*. *Journal of Alloys and Compounds*[J], 2024, 976: 173279
28 Wang Z J, Guo S, Liu C T. *JOM*[J], 2014, 66(10):1966
29 Qi L, Chrzan D C. *Physical Review Letters*[J], 2014, 112(11): 115503
30 Sheikh S, Shafeie S, Hu Q *et al*. *Journal of Applied Physics*[J], 2016, 120(16): 164802
31 Yao H W, Qiao J W, Hawk J A *et al*. *Journal of Alloys and Compounds*[J], 2017, 696: 1139

Ti元素对NbTaMoWTi$_x$难熔高熵合金组织、性能及热稳定性的影响

欧鹏程[1]，万　强[1]，姜　慧[2]，沙明红[1]，孙嘉彬[1]，艾新港[1]，李胜利[1]，黄天荡[1]
(1. 辽宁科技大学 材料与冶金学院，辽宁 鞍山 114051)
(2. 青岛大学 机电工程学院，山东 青岛 266000)

摘　要：研究了Ti元素对NbTaMoWTi$_x$ (x=0, 1, 1.5, 2) 难熔高熵合金铸造态和退火态组织和力学性能的影响。结果表明：加入Ti后，铸造态合金仍然保持原有的体心立方（bcc）结构；力学性能方面，对比未加入Ti元素的NbTaMoW合金，强度和塑性分别提高了93%和215%。NbTaMoWTi$_x$合金表现出优异的热稳定性。在经过1400 ℃退火处理后，仍然可以保持bcc单相结构，力学性能甚至略有提升。然而，高Ti含量合金（NbTaMoWTi$_{1.5}$与NbTaMoWTi$_2$）经过退火处理后，由于富Ti针状相的出现，力学性能明显下降。

关键词：高熵合金；难熔合金；钛；力学性能；热稳定性

作者简介：欧鹏程，男，2003年生，辽宁科技大学材料与冶金学院，辽宁 鞍山 114051，E-mail：120223205093@ustl.edu.cn